AGU PUBLICATIONS

JGR

Journal of Geophysical Research: Biogeosciences

RESEARCH ARTICLE
10.1002/2017JG004145

Key Points:
- A new conceptual model of microwave vegetation optical depth dynamics in terms of leaf area index and leaf water potential was developed
- The conceptual model was validated using leaf water potential measurements at two mixed deciduous forests and a pinion-juniper woodland
- Globally, the suggested framework increased the correlation of water potential (leaf area index) with observed VOD by ~30% (~15%)

Supporting Information:
- Supporting Information S1

Correspondence to:
M. Momen,
mymomen@gmail.com

Citation:
Momen, M., Wood, J. D., Novick, K. A., Pangle, R., Pockman, W. T., McDowell, N. G., & Konings, A. G. (2017). Interacting effects of leaf water potential and biomass on vegetation optical depth. *Journal of Geophysical Research: Biogeosciences*, *122*, 3031–3046. https://doi.org/10.1002/2017JG004145

Received 8 SEP 2017
Accepted 26 OCT 2017
Accepted article online 6 NOV 2017
Published online 23 NOV 2017

Interacting Effects of Leaf Water Potential and Biomass on Vegetation Optical Depth

Mostafa Momen[1], Jeffrey D. Wood[2], Kimberly A. Novick[3], Robert Pangle[4], William T. Pockman[4], Nate G. McDowell[5], and Alexandra G. Konings[1]

[1]Department of Earth System Science, Stanford University, Stanford, CA, USA, [2]School of Natural Resources, University of Missouri, Columbia, MO, USA, [3]School of Public and Environmental Affairs, Indiana University—Bloomington, Bloomington, IN, USA, [4]Department of Biology, University of New Mexico, Albuquerque, NM, USA, [5]Pacific Northwest National Laboratory, Richland, WA, USA

Abstract Remotely sensed microwave observations of vegetation optical depth (VOD) have been widely used for examining vegetation responses to climate. Nevertheless, the relative impacts of phenological changes in leaf biomass and water stress on VOD have not been explicitly disentangled. In particular, determining whether leaf water potential (ψ_L) affects VOD may allow these data sets as a constraint for plant hydraulic models. Here we test the sensitivity of VOD to variations in ψ_L and present a conceptual framework that relates VOD to ψ_L and total biomass including leaves, whose dynamics are measured through leaf area index, and woody components. We used measurements of ψ_L from three sites across the US—a mixed deciduous forests in Indiana and Missouri and a piñon-juniper woodland in New Mexico—to validate the conceptual model. The temporal dynamics of X-band VOD were similar to those of the VOD signal estimated from the new conceptual model with observed ψ_L (R^2 = 0.6–0.8). At the global scale, accounting for a combination of biomass and estimated ψ_L (based on satellite surface soil moisture data) increased correlations with VOD by ~ 15% and 30% compared to biomass and water potential, respectively. In wetter regions with denser and taller canopy heights, VOD has a higher correlation with leaf area index than with water stress and vice versa in drier regions. Our results demonstrate that variations in both phenology and ψ_L must be considered to accurately interpret the dynamics of VOD observations for ecological applications.

1. Introduction

Remote sensing of vegetation is useful for monitoring ecosystem health, identifying trends in vegetation characteristics, and developing an improved understanding of global carbon and water cycles (Jones & Vaughan, 2010). Among remotely sensed vegetation indices, microwave radiometry-derived observations of vegetation optical depth (VOD) have been widely used to study trends in biomass (Liu et al., 2015) and woody encroachment (Brandt et al., 2017). VOD is a dimensionless parameter that describes the rate of attenuation of microwaves as they pass through the vegetation canopy. This attenuation rate depends on both canopy structure and vegetation water content (Jackson & Schmugge, 1991; Wigneron et al., 2004). Depending on the application, different VOD data sets have been alternately interpreted as predominantly sensitive to vegetation biomass (Guan et al., 2014; Liu et al., 2013, 2015; Tian et al., 2017), or some unspecified combination of biomass and water content (e.g., Andela et al., 2013; Jones et al., 2012, 2013). Because of its integrated sensitivity to both vegetation density and water content, VOD has also been used as a proxy for fuel loads (Forkel et al., 2016; Tian et al., 2017). However, the relative sensitivity of VOD to vegetation density and water content is poorly defined in most studies limiting its utility.

Both theoretical considerations and field experiments in grassy and shrubby vegetation types have shown a linear relationship between VOD and the vegetation water content (VWC) of the canopy (i.e., the mass of canopy water; Jackson & Schmugge, 1991). More recently, satellite-based products have been validated by comparison to herbaceous and woody biomass components in the Sahel (Tian et al., 2016). Microwaves attenuate as they pass through vegetation, such that space-based observations are generally most sensitive to the upper canopy. The relative sensitivity to different canopy layers varies with canopy structure and electromagnetic frequency (more sensitive to lower layers at lower frequency; Ulaby & Long, 2014). At lower L-band frequencies, VOD has also been shown to carry information about crop growth and yield (Hornbuckle et al., 2016). Space-based VOD data sets from a number of different sources (sensor

instrument, operating frequency, and retrieval algorithm) have been compared extensively to optically derived vegetation indices, including the normalized difference vegetation index (NDVI) and leaf area index (LAI; Du et al., 2017; Jones et al., 2011; Lawrence et al., 2014; Liu, De Jeu, et al., 2011; Tian et al., 2016).

Despite extensive validation of the relationship between satellite-derived VOD estimates and vegetation density, relatively few studies have explicitly sought to validate the sensitivity of VOD to canopy water status. The relative water content of a canopy is proportional to leaf water stress (Bartlett et al., 2012). Given the increasing availability (Du et al., 2017; Fernandez-Moran et al., 2017; Konings et al., 2016; Konings, Piles, et al., 2017; Liu, De Jeu, et al., 2011), length, and use of new VOD data sets, it is crucial to better understand how water stress affects VOD to properly interpret the signal. Microwave remote sensing indices such as VOD have the potential to be particularly useful for studies of water stress because they are much less sensitive to atmospheric conditions and sun-sensor geometry than optical or hyperspectral sensors (Morton et al., 2014; Ulaby et al., 1982) and are available even during cloudy conditions. Understanding the effect of water stress on VOD is also needed for investigating the interpretations of changes in VOD that are solely attributed to biomass changes.

Studies of vegetation water stress often consider the dynamics of leaf water potential (ψ_L), which has long been known to plant physiologists to reflect plant hydraulic status, and is strongly linked to stomatal closure and xylem embolism (Jarvis, 1976; Sperry & Tyree, 1988). During periods of negligible transpiration, ψ_L is often assumed to be equilibrated with soil water potential (Donovan et al., 2003). During daytime periods, it will decline to create the driving force necessary to move water from the soil to the leaves. Plants regulate ψ_L by reducing stomatal conductance to prevent excessively negative ψ_L that can damage xylem. The incorporation of plant hydraulics in dynamic global vegetation models and earth system models is becoming increasingly common (Bonan et al., 2014; Christoffersen et al., 2016; Matheny et al., 2017; Xu et al., 2016), and the ability to constrain ψ_L with remotely sensed observations would be particularly useful for benchmarking and parameterizing these models. Furthermore, these inferred constrained ecohydrological parameters could be useful for improving the accuracy of atmospheric boundary layer models (e.g., Momen & Bou-Zeid, 2016, 2017) by providing realistic boundary conditions for such flows. While diurnal variations in VOD have previously been assumed to be indicative of changes in ψ_L (Konings & Gentine, 2017; Konings, Williams, et al., 2017), the sensitivity of VOD to ψ_L has not been explicitly tested.

In this paper, we aim to relate VOD to a combination of ψ_L and total biomass (leaves and stems/branches). In particular, we seek to better understand the factors affecting VOD by addressing the following research questions:

1. How can we disentangle the sensitivity of VOD to ecosystem-level leaf water potential and aboveground biomass (AGB)?
2. What are the relative and interacting effects of leaf water potential and total AGB (phenological and static biomass) on VOD across ecosystems, and how well do they capture observed VOD variability?

To address question 1, we introduce a new conceptual framework that incorporates the interacting effects of water potential and canopy biomass in section 2.1. Next, we describe the used data sets and the analyses in section 2.2. In section 3, the validity of this conceptual model will be examined using measurements of ψ_L. Leaf water potential is a challenging variable to measure at a high temporal frequency, as it requires access to canopy leaves that are often dozens of meters above the ground surface. Here we leveraged three preexisting high-frequency ψ_L data sets from three forested sites in the United States that span a broad range of climate conditions and species. Finally, remotely sensed surface soil moisture was used to estimate ψ_L at the global scale to better examine variations in the relative roles of water status and phenology across ecosystems in section 4.

2. Methods

2.1. Conceptual Model

VOD is expected to be linearly proportional to VWC (in units of mass of water per unit area) in a canopy (Jackson & Schmugge, 1991):

$$\mathrm{VOD} = b \times \mathrm{VWC}, \tag{1}$$

where b depends on canopy structure. Note that some studies of lower frequency (L-Band) VOD showed that b may also depend on time and decrease during senescence (likely due to changes in vegetation structure); however, such dependence on time was found to be relatively low (Wigneron et al., 2004), and so we consider a time-constant value of b here. The VWC is the product of the total aboveground dry biomass per unit area (AGB) and the relative water content (RWC; mass of water per unit mass of dry AGB) as

$$\mathrm{VWC} = \mathrm{AGB} \times \mathrm{RWC}. \tag{2}$$

We considered total vegetation mass as the sum of a static component that does not change significantly within a year, represented as s (stems and branches), and a dynamic component that was dependent on leaf phenology. The latter term is assumed to be proportional to the leaf area index, $\mathrm{AGB}_{\mathrm{leaf}} = p \times \mathrm{LAI}$, where p is a constant of proportionality that may vary in space across canopies, but does not vary in time. Hence, total AGB can be written as

$$\mathrm{AGB} = p\mathrm{LAI} + s. \tag{3}$$

Note that the growth of woody plant components over time is neglected in this model. Over the seasonal-scale analyses performed in section 3.1, the effect of woody plant growth is assumed to be negligible, although it can be significant at multiyear timescales such as the 8 year record used in section 3.2. We expect that any variation in VOD due to growth of the woody components over the longer record used in section 3.2 will be partially reflected in the LAI (because larger trees support more leaf area) and will primarily affect the value of p (which is not studied in this paper), minimizing the errors associated with this assumption. Consideration of both the woody and leafy components in equation (3) is consistent with previous findings that VOD signals at frequencies higher than 6.8 GHz include the effects of water content both in herbaceous and woody plant leaves/stems (Guglielmetti et al., 2007; Santi et al., 2009; Tian et al., 2017).

At the individual scale, the RWC of different plant components has been related to their ψ_{L}. Direct measurements of changes in water content in different plant (crowns and stems) components have been linked to water potential in these components using laboratory measurements of Norway spruce saplings (Zweifel et al., 2000, 2001). RWC is usually related to ψ_{L} using a pseudo-exponential Weibull function (Pearcy et al., 1989; Zweifel et al., 2000). Here we linearize this relationship and write

$$\mathrm{RWC} = m\psi_{\mathrm{L}} + n, \tag{4}$$

where n (mass of water per unit mass of dry AGB) is the intercept of this linearization, which represents RWC when $\psi_{\mathrm{L}} = 0$, and m (mass of water per unit mass of dry AGB over MPa) is the slope of this relationship. This assumption of linearity between RWC and ψ_{L} has previously been used to determine the degree of ecosystem isohydricity across the globe based on X-band VOD (Konings & Gentine, 2017) and is consistent with similar assumptions regarding linearity between xylem conductivity loss and ψ_{L} (also often modeled as a Weibull function) in modeling studies (Gentine et al., 2015; Manzoni et al., 2014). Equation (4) further implicitly assumes that leaf and xylem water potential are equal, which may not be the case, particularly for trees with high stem water storage (Köcher et al., 2013; Phillips et al., 2003). Combining equations (1–4) gives

$$\mathrm{VOD} = b(m\psi_{\mathrm{L}} + n)(p\mathrm{LAI} + s) = \alpha + \beta\mathrm{LAI} + \gamma\psi_{\mathrm{L}} + \eta\psi_{\mathrm{L}}\mathrm{LAI}, \tag{5}$$

where α is the intercept and β, γ, and η are the slopes of the multiple linear conceptual model that do not vary with time but vary in space. Based on this conceptual model, VOD depends on LAI, ψ_{L}, and their interaction. The parameters of this linear relationship vary in space and are difficult to estimate a priori. In this paper, we focus on whether the conceptual model can capture the dynamics of observed VOD, rather than on predicting the static parameters of equation (5). We attempt to estimate a best-fit VOD proxy, referred as $\mathrm{VOD}_{\mathrm{est.}}$ here, by regressing against site-specific observations (in section 3) and global estimates (in section 4) of LAI and ψ_{L} using the functional form of equation (5). The conceptual model is judged based on the ability of the $\mathrm{VOD}_{\mathrm{est.}}$ obtained from regression to capture the observed VOD.

2.2. Analyses and Data Sets

In this paper, we focus on VOD data sets obtained at X-band frequency, because this frequency is more sensitive to canopy leaves (rather than stems or understory) than observations at lower frequencies and because longer observational records are available compared to other frequency bands. The Land Parameter Retrieval Model (Meesters et al., 2005; Owe et al., 2008) was used to retrieve VOD from X-band observations obtained

Table 1
Description of the Observational Data Sets of ψ_L

	Name	Latitude, longitude	Years	ψ_L observation time	Mean annual precipitation	Vegetation type
1	Sevilleta	34.4°N, 106.5°W	2007–2014	Predawn	360 mm	Woodland
2	Missouri Ozarks AmeriFlux (MOFLUX)	38.7°N, 92.2°W	2004–2010	Predawn	1,080 mm	Mixed deciduous forest
3	Morgan–Monroe State Forest AmeriFlux	39.25°N, 86.5°W	2012–2013	Midday	1,030 mm	Mixed hardwood forest

by the JAXA Advanced Microwave Scanning Radiometer—Earth Observing System (AMSR-E). In late 2011, AMSR-E ceased operations, after which retrievals from the Advanced Microwave Scanning Radiometer-2 (AMSR2) were used instead (Parinussa et al., 2015). Although the two sensors were designed to be similar, some minor biases between these two data sets may remain due to calibration differences (Du et al., 2014). To reduce the effect of this bias, only AMSR-E data are used in the global analyses. For the local-scale comparison, only one site (Sevilleta) spanned across the two sensors, although the results did not appear sensitive to the sensor used (see section 3.1). Furthermore, to reduce the effect of canopy-intercepted water from rainfall on VOD (Saleh et al., 2006), all observations on days with precipitation were removed. We assume that most intercepted canopy-water evaporates within 1 day, so that nonrainy days are free of canopy interception errors. Precipitation data were obtained from the TRMM 3B42RT product (Huffman et al., 2007) to match the VOD resolution of 0.25°. Note that TRMM data are not available above 50°N and below 50°S. Therefore, rainy days were not removed from the analysis above 50°N. Since filtering rainy days elsewhere had only a minor quantitative effect on the global analyses (see section 4), we do not expect this to significantly influence the results. Furthermore, conditions when the land surface temperature is less than 273°K are assumed to represent frozen soil and were removed from this analysis.

The Global Land Surface Satellite (GLASS) data set was used for LAI (Liang & Xiao, 2012; Xiao et al., 2014). It is based on a neural network approach applied to reflectance from the Moderate-Resolution Imaging Spectroradiometer (MODIS) instrument onboard the Terra satellite. The LAI data set is linearly averaged from a 0.05° to 0.25° resolution to match the VOD observations. Consistent with other MODIS products, the temporal resolution of LAI data is 8 days because of observing limitations in the presence of cloud cover. The VOD daily data are averaged to match this 8 day temporal resolution for consistency.

2.2.1. Local-Scale Observations

Observational data sets of ψ_L from three sites were used for validation purposes. The description of these data sets is shown in Table 1. Sevilleta is located at the base of eastern flank of the Los Pinos Mountains in New Mexico and is significantly less than at the other sites considered. The site is a woodland dominated by two species: piñon pine (*Pinus edulis*, Engelm. with average height of 2.8 m and average crown area of about 1,170 m^2 ha^{-1}) and juniper (*Juniperus monosperma Sarg*., with average height of 2.7 m and average crown area of about 2,635 m^2 ha^{-1}), with few other commonly observed shrub species. Several drought treatments were applied in the study that generated these data, but only ambient control data are used here to increase representativeness compared to the greater VOD pixel. The canopy average for Sevilleta was calculated based on crown area. See (Plaut et al., 2012) for additional information about the site and the measurements.

Missouri Ozarks AmeriFlux (MOFLUX) is located in the University of Missouri's Baskett wildlife Research and Education Center. It is a mixed deciduous forest (oak-hickory) located in a warm, humid, and continental climate with mean annual temperature of 12.6 °C; and with monthly mean minimum and maximum temperatures of −1.3°C (January) and 25.2°C (July; National Centers for Environmental Information, 1981–2010 Climate Normals). The upper quartile of canopy tree heights has a mean of 22 m (Gu et al., 2016), and the stand age is 80–90 years. On each sampling, a total of 20–21 leaves were collected before dawn, with 6–7 taken from white oak (*Quercus alba* L.) and the rest distributed among other major species approximately proportional to their relative dominance in the stand. Details of the predawn ψ_L sampling methods are given in (Gu et al., 2015). The tree species sampled included: white oak (~39% of basal area), eastern redcedar (*Juniperus virginiana* L., ~10% of basal area), black oak (*Q. velutina* Lam. about 9% of basal area), shagbark hickory (*Carya ovata* (Mill.) K. Koch, ~7% of basal area), and sugar maple (*Acer saccharum* Marsh., ~7% of basal area). The canopy-scale average predawn ψ_L was estimated as the average, weighted by basal area.

Morgan–Monroe State Forest AmeriFlux is located in a mixed hardwood forest in south-central Indiana, USA (39.25°N, 86.5°W; Schmid et al., 2000). For each sampling week during the growing seasons of 2012 and 2013, 120 leaf samples were collected at midday, spanning 12 trees, 5 leaves from each tree, and 2 canopy positions (Roman et al., 2015). During this time period, the site experienced a severe drought event that promoted significant variation in midday leaf water potential, both in time and across species. The dominant sampled tree species of this site are sugar maple (~38% of litter LAI) and tulip poplar (*Liriodendron tulipifera*, ~11% of litter LAI), and the observations of sunlit and shaded leaves were averaged for both species. At this site, the canopy-average midday leaf water potential was calculated based on a weighting by fractional LAI determined from litter-fall measurements as described in Roman et al. (2015). The average height of the trees is 27 m, and the average age of the trees is 80–90 years.

Leaf samples were collected before dawn at both MOFLUX and Sevilleta and compared to VOD observations at a local overpass time of 1:30 AM. The midday samples of ψ_L at Morgan–Monroe were compared to VOD observations at 1:30 PM. The footprint of the VOD observations is several orders of magnitude larger than that represented by the ψ_L observations, and furthermore, each pixel includes a number of land-cover types. Because repeated microwave observations at finer resolutions are not available, comparison across this large range of resolution was necessary (see further discussion below).

2.2.2. Global Scale Observations

The three local-scale sites cover a limited range of ecosystem types. Hence, we attempted to examine the conceptual model at the global scale. Since ψ_L observations are not available across the globe, remotely sensed soil moisture observations were used a separate proxy of water availability. Soil moisture retrievals from the European Space Agency Climate Change Initiative (CCI) active-passive soil moisture data set are used (Liu, Parinussa, et al., 2011b; Liu et al., 2012; Wagner et al., 2012). This product combines soil moisture retrievals from multiple satellites by rescaling them to a common model climatology and using a weighted average based on expected error statistics for each satellite and location. Soil type information from the Harmonized World Soil Database (Fischer et al., 2010) was employed for converting the soil moisture data to soil water potential, ψ_s. In this paper, a regridded version of the soil database product was used (Wieder et al., 2012).

We use surface soil moisture data as a surrogate to investigate the variation in predawn ψ_L by employing the following procedure:

1. Remotely sensed surface soil moisture observations are used to derive surface soil water potential ($\psi_{s,surf}$, using empirical pedotransfer functions based on (Brooks & Corey, 1964)—see supporting information text S1). The results were qualitatively robust to using alternative pedotransfer functions.
2. We assumed the variability of the surface remote-sensing $\psi_{s,surf}$ is proportional to the variability of the root-zone ψ_s, that is, that $\psi_{s,surf}(t)$ is proportional to $\psi_{s,root\text{-}zone}(t)$. Variations in soil moisture with depth due to flow in the unsaturated zone and depth-dependent root water uptake ensure that this assumption is likely a cause of error. Nevertheless, we assume that the surface soil water still provides some information about root-zone water dynamics and how they may differ from the dynamics of leaf area
3. We assumed that at the 1:30 AM local time of the VOD overpass, leaf and root-zone water potentials are in equilibrium; hence, $\psi_{s,root\text{-}zone}(t)$ is proportional to $\psi_L(t)$. That is, we assume that the nighttime rehydration of leaf water potential—which brings it into equilibrium with the soil (Boyer, 1967; Herrera et al., 2008; Larcher, 1995)—is largely completed by 1:30 AM. Nighttime transpiration or insufficiently fast refilling rates for some or all of the species in a pixel cause this to be an imperfect assumption (Donovan et al., 2003).

These three assumptions allowed us to approximate the temporal dynamics of $\psi_L(t)$ at the global scale as $\psi_L^{est.}(t) = \psi_s(t)$. The resulting variable is referred to as $\psi_L^{est.}$ below. Despite the facts that our estimates of $\psi_L^{est.}$ have several potential sources of error, they are expected to capture the dynamics of ψ_L to zeroth-order, such that they can still be informative about the relative sensitivities of VOD. Pixels with annual average LAI less than 0.05 or which are covered by tropical forests—in which soil moisture retrievals are not possible because the dense vegetation prevents the electromagnetic waves from penetrating to the soil (Liu et al., 2012)—were removed from the analysis. In addition, pixels for which more than 75% of possible data points were missing (either due to a lack of overpasses or filtering of rainy days) were removed.

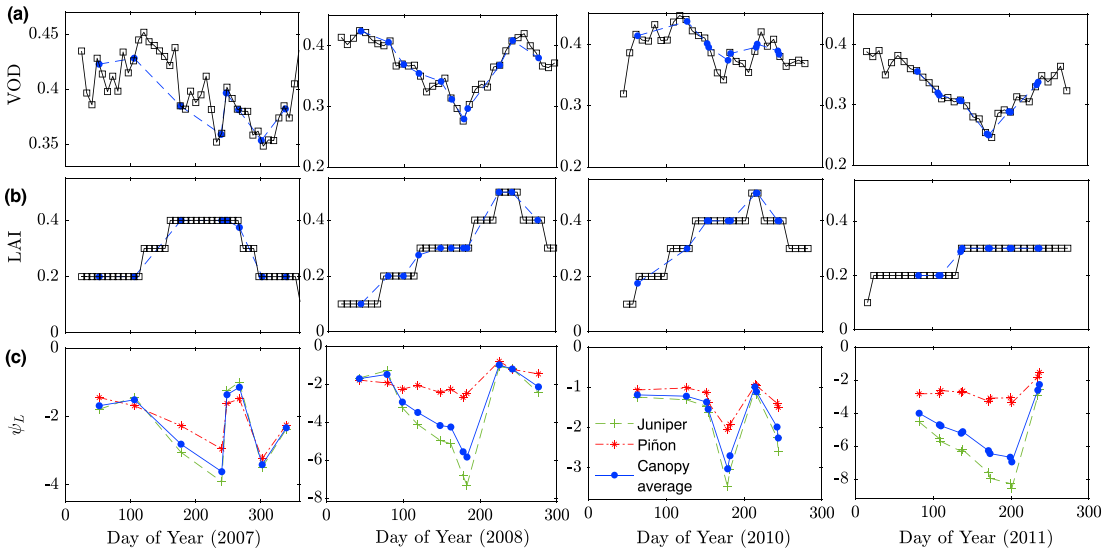

Figure 1. Time series of (a) $VOD_{midnight}$, (b) LAI, and (c) predawn leaf water potential (ψ_L) at the Sevilleta site in New Mexico for 4 years with high numbers of available measurements: 2007, 2008, 2010, and 2011. In Figures 1a and 1b, the satellite-derived observations are shown as black squares for each 8 day period, while blue dots represent values that are linearly interpolated to match the dates of the ψ_L measurements. The canopy average ψ_L is based on the average crown area sizes of piñon pine (asterisks) and juniper (plus signs).

To determine the relative contribution of LAI and ${\psi_L}^{est.}$ to $VOD_{est.}$, partial correlations were calculated. The partial correlations for three variables are defined as below:

$$R\left(\mathrm{VOD},\mathrm{LAI}:\psi_L^{est.}\right)=\frac{R(\mathrm{VOD},\mathrm{LAI})-R\left(\mathrm{VOD},\psi_L^{est.}\right)R\left(\psi_L^{est.},\mathrm{LAI}\right)}{\sqrt{1-R\left(\mathrm{VOD},\psi_L^{est.}\right)^2}\sqrt{1-R\left(\psi_L^{est.},\mathrm{LAI}\right)^2}}, \tag{6a}$$

$$R\left(\mathrm{VOD},\psi_L^{est.}:\mathrm{LAI}\right)=\frac{R\left(\mathrm{VOD},\psi_L^{est.}\right)-R(\mathrm{VOD},\mathrm{LAI})R\left(\mathrm{LAI},\psi_L^{est.}\right)}{\sqrt{1-R(\mathrm{VOD},\mathrm{LAI})^2}\sqrt{1-R\left(\mathrm{LAI},\psi_L^{est.}\right)^2}}, \tag{6b}$$

where equation (6a) represents the partial correlation between VOD and LAI and equation (6b) shows the partial correlation between VOD and ${\psi_L}^{est.}$.

Several ancillary data sets were used to aid in the interpretation of results. These included canopy height determined from space-based lidar observations made by the Geoscience Laser Altimeter System (GLAS) aboard the NASA Ice, Cloud, and Land Elevation satellite (ICeSat; with a regression tree used to fill in locations with missing data; Simard et al., 2011) and land-cover type data from the MODIS MCD12C1 product (Friedl et al., 2010). Both data sets are linearly averaged to match the 0.25° resolution of the VOD data.

3. Results

3.1. Local Validation Against Ground-Based Measurements

At all three evaluation sites, the temporal variability of VOD was compared with the temporal variability of canopy-averaged ψ_L and LAI. The temporal variability of two dynamic variables in the conceptual model of VOD—LAI and ψ_L—are provided for each of the three study sites in Figures 1–3. At each site, a constrained multilinear regression was performed to validate the conceptual model.

In the sparsely vegetated Sevilleta site, LAI is relatively low and is poorly correlated with VOD. By contrast, VOD clearly follows the dynamics of the canopy-average ψ_L (R^2 = 0.77, Figure S1). Four of the 8 years of available data at Sevilleta, NM are provided in Figure 1. Although only 4 years are shown here for clearer visual interpretation, the other years displayed qualitatively similar dynamics. The dominant species at this site are evergreen, thus permitting measurements of ψ_L throughout the entire year. The two dominant species at this site have very different hydraulic strategies. The piñon pines are isohydric and therefore maintain a

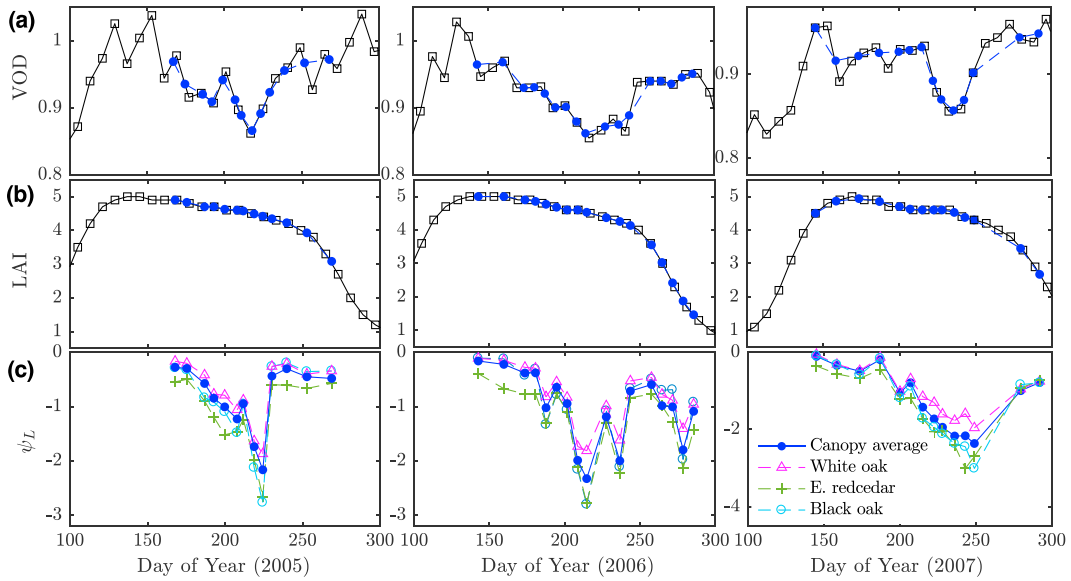

Figure 2. Time series of (a) $VOD_{midnight}$, (b) LAI, and (c) predawn leaf water potential (ψ_L), at the MOFLUX site in Missouri for 2005–2007. In Figures 2a and 2b, the satellite-derived observations are shown as black squares for each 8 day period, while blue dots represent values that are linearly interpolated to match the dates of the leaf water potential (ψ_L) measurements. The canopy average ψ_L was based on the basal area of trees. Three dominant species are shown: White oak (38.9% of basal area), eastern redcedar (9.7% of basal area), and black oak (9.4% of basal area).

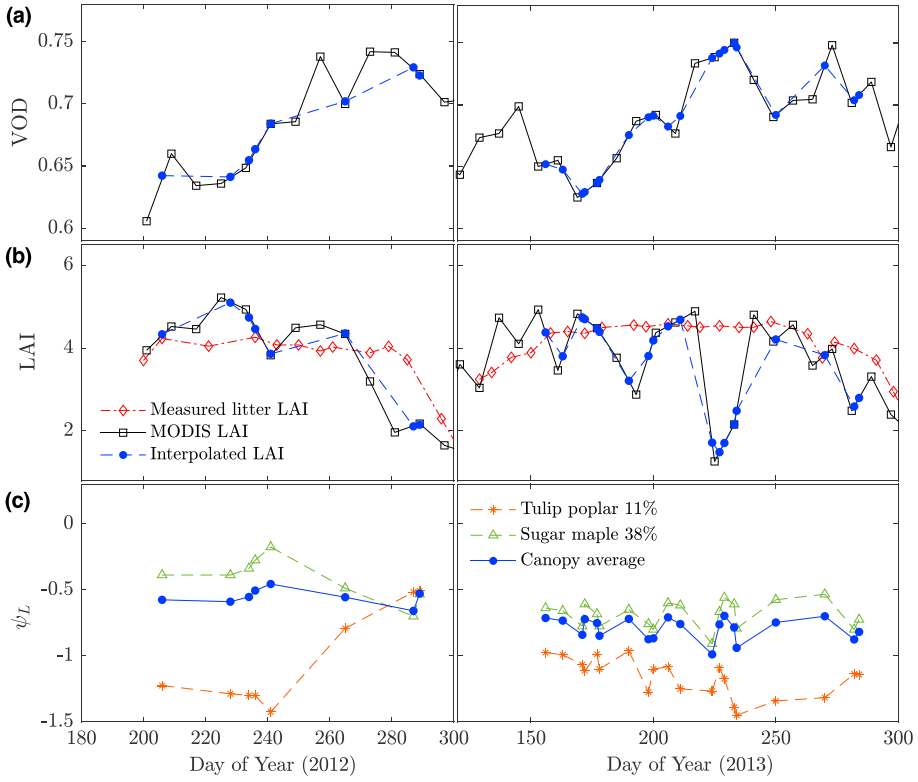

Figure 3. Time series of (a) VOD_{midday}, (b) LAI, and (c) midday leaf water potential (ψ_L), at the Morgan–Monroe site for 2012–2013. In Figures 3a and 3b, the satellite-derived observations are shown as black squares for each 8 day period, while blue dots represent values that are linearly interpolated to match the dates of the ψ_L measurements. The canopy average ψ_L was based on the litter LAI measurements shown in Figure 3b.

relatively constant ψ_L (as observed, green line in Figure 1c), while the ψ_L of the anisohydric juniper is more variable. The juniper species are more dominant at this site, with a crown area of 2,635 m^2 ha^{-1} instead of 1,170 m^2 ha^{-1} for the pines. Consistent with its relative dominance as a species, the dynamics of VOD are more influenced by juniper ψ_L than for piñon pines, as can be seen by comparing the relative magnitude of the midseason decline in VOD compared to the difference between the early season and late season values. Furthermore, a number of other species (e.g., grasses) also have nearby habitats within the 25 × 25 km VOD pixel. Indeed, within the greater 0.25° pixel covered by VOD, MODIS classifies 37% of the areas as grasslands and 60% as open shrublands. The close similarity between the VOD and the woody canopy-average ψ_L suggests that the grassy species contribute relatively little to the VOD data at Sevilleta or that the canopy-average of grass water potential dynamics is similar to the weighted average of the two tree species.

At the MOFLUX site in Missouri, the predawn ψ_L of three of the dominant species (white oak, eastern red-cedar, and black oak—together comprising ~58% of the canopy basal area) follow fluctuations similar to the VOD (R^2 = 0.53). Although the LAI at the MOFLUX site in Missouri is much higher than at Sevilleta, its variability during the peak growing season (when most ψ_L measurements were made, as sufficient numbers of the leaves must be available for measurements) is relatively limited until after about DOY 250 (Figure 2). Thus, it is not surprising that the VOD dynamics at this site once again resemble the measured predawn ψ_L more closely than LAI before DOY 250 in each year. However, even after LAI declines in late 2007, VOD continues to follow the dynamics of ψ_L more closely than those of LAI. By contrast, the ψ_L and LAI of all dominant species both decline after about DOY 260 in 2006, but VOD does not. It is tempting to attribute this difference to heterogeneity across the VOD pixel, for example, to contributions from soybean and corn agricultural areas (~9% of the pixel is covered with croplands based on the MODIS data) that cover a minority of the VOD pixel but whose ψ_L dynamics may differ from those of the forests. However, based on our tests, the correspondence between VOD and the conceptual model was not significantly worse during only times of peak agricultural biomass (R^2 = 0.62, p value $<$ 0.001) than the whole measurement period (R^2 = 0.64, p value $<$ 0.001) including times before the peak agricultural growing season (July, ~DOY 182) or after harvest (September and on, ~DOY 274). Hence, the late 2006 VOD behavior may be due to VOD retrieval errors, heterogeneity within the forested regions of the pixel, or other sources of error (see Section 5).

Unlike at Sevilleta and MOFLUX, ψ_L measurements at the Morgan–Monroe site were collected at midday rather than predawn. Therefore, afternoon (local time 1:30 PM) rather than early morning (local time 1:30 AM) VOD observations are used for comparison. Two years of data from the Morgan–Monroe site are depicted in Figure 3. The AMSR2 instrument whose VOD retrievals are used in the 2012–2013 period did not become fully operational until the second half of 2012, leading to a lower number of data points in 2012 than 2013. Note that the MODIS-derived LAI showed large fluctuations at Morgan–Monroe. Although these are included in Figure 3 for consistency with other sites, additional LAI observations based on litter are also shown (in red). Afternoon VOD retrievals may be more prone to error than nighttime ones due to the lack of thermal equilibrium between canopy and soil temperatures (a common assumption in the retrieval of VOD from observed brightness temperatures). Perhaps partially because of these data quality issues, the VOD variability in Figure 3 is less correlated to that of ψ_L (R^2 = 0.1, p value = 0.08 for the whole Morgan–Monroe data set) than for other sites. At Morgan–Monroe, time-averaged leaf litter-derived LAI values for the two dominant species (Roman et al., 2015; Schmid et al., 2000) were used to estimate a canopy-average estimate of ψ_L.

To test the sensitivities of VOD to LAI and ψ_L quantitatively, we attempted to estimate the observed VOD dynamics using the conceptual model (equation (5)) and the available observational data for three sites, shown in Figures 1–3. We randomly shuffle and split our data sets into a training (calibration—80% of the data) and a testing (evaluation—20% of the data) subset. Specifically, we regressed VOD against MODIS LAI data and site-level ψ_L measurements based on the functional form of the conceptual model in equation (5) for the training subset. Note that the static coefficients of the conceptual model (i.e., α, β, γ, and η) in equation (5) must be nonnegative because the m, n, s, and p parameters represent physical quantities that have nonnegative values. Hence, a constrained multiple linear regression approach that restricts the coefficients to be nonnegative was used for the regression. The best-fit values were used for the static

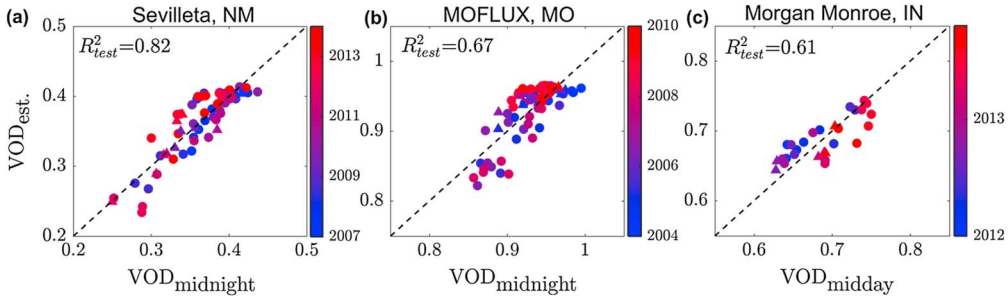

Figure 4. Local validation of the estimated VOD using the conceptual model against field measurements employing a constrained multiple linear regression for (a) Sevilleta ($\alpha = 0.45, \beta = 0, \gamma = 0.02, \eta = 0.03$), (b) MOFLUX ($\alpha = 0.97, \beta = 0, \gamma = 0.01, \eta = 0.02$), and (c) Morgan–Monroe ($\alpha = 0.84, \beta = 0.01, \gamma = 0.01, \eta = 0.04$). Note that AMSR-E VOD data are used in Figure 4b, AMSR2 VOD observations are employed in Figure 4c, and in Figure 4a VOD data from both AMSRE (2007–2011) and AMSR2 (2012–2014) are used. The blue-red colors show years, the circles show the trained data, and triangles represent the test data, which are only used for validation.

coefficients at each site, as values for these parameters are difficult to estimate a priori and because here we focus on dynamical variables (VOD, LAI, and ψ_L) rather than these constant coefficients. The coefficients found from the training subset are then used to evaluate the model's performance using the testing subset. The regression results are shown in Figure 4 for each of the three sites, in which the test subsets are masked with a gray color. At all sites, the conceptual model reproduced observed VOD dynamics reasonably well given the uncertainties associated with the scale mismatch between data sets (R^2_{test} = 0.61–0.82, p values < 0.001). The residuals are independent of the time of the record, implying a constant relationship between VOD and tree characteristics at each site. Furthermore, since the conceptual model combines the biomass and water stress effects, it outperformed the correlations of VOD with those terms individually (Table 2 and Figure S1). Indeed, if only LAI is used in the regression, no more than 5% of the observed variability of VOD during growing season can be explained (Table 2).

Despite the location of the ψ_L observations being arguably less representative of the VOD pixel at Sevilleta than at MOFLUX and Morgan–Monroe, the estimated VOD is most successful in explaining observed VOD variability there. This could be due to either the lower number of dominant species there (2 versus 5–10) or the fact that the nonwooded areas of this VOD pixel are composed of grasses and shrubs that contribute relatively little to the overall VOD signal, unlike the agricultural, urban, and understory contributions that affect the VOD at MOFLUX and Morgan–Monroe. Lastly, the Morgan–Monroe and MOFLUX sites contain far more plant water than the Sevilleta site and may be more sensitive to nonlinearities in the ψ_L–RWC content relationship (equation (4)) due to the effects of stem water storage.

The intercept of the conceptual model is proportional to the temporally constant dry biomass of the woody components such as stems and branches (parameter s in equation (5)) in the reconstructed VOD signal. We therefore expect its regression-based value to be high in taller canopies. This can be tested across the tree sites. The intercept values of Morgan–Monroe and MOFLUX sites (α = 0.84, standard error = 0.09, and α = 0.97, standard error = 0.03, respectively) are about twice as high as that of the Sevilleta site (α = 0.45, standard error = 0.02). This trend is consistent with the average canopy height in those two sites (≈27 m at Morgan–Monroe and ~20 m at MOFLUX), compared to the Sevilleta average canopy height, ≈3 m. This relation will be explicitly investigated at a global scale for all the available pixels in the next section.

Table 2
Local-Scale Correlation Analysis for Three Studied Sites—Test Subset

Coefficient of determination	Sevilleta	MOFLUX	Morgan–Monroe
R^2_{test} (VOD, $VOD_{est.}$)	0.82	0.67	0.61
R^2_{test} (VOD, $\alpha + \beta$ LAI)	0.05	0.02	0.02
R^2_{test} (VOD, $\alpha + \gamma \psi_L$)	0.81	0.60	0.08
R^2_{test} (VOD, $\alpha + \eta \psi_L$LAI)	0.71	0.67	0.58

3.2. Global Validation Against Remote Sensing Data

The three sites studied in section 3 cover a limited range of ecosystem types. Here we examined the relative contribution of AGB and ψ_L on the VOD signal at a global scale and across ecosystems in various climatic regions. We also evaluated the conceptual VOD reconstruction framework at the global scale.

Using the VOD signal at the global scale based on the conceptual model, remotely sensed LAI data, and estimated values of ψ_L (obtained via the

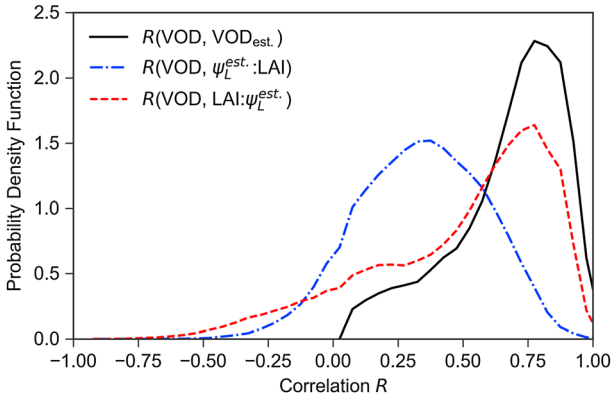

Figure 5. The probability density function of the correlation between VOD and $VOD_{est.}$ (black solid line), the partial correlation between VOD and $\psi_L^{est.}$, accounting for LAI (red dashed line), and the partial correlation between VOD and LAI, accounting for $\psi_L^{est.}$ (blue dash-dotted line) during 2003–2010.

soil moisture data), we found that the correlation of VOD with LAI is higher than with $\psi_L^{est.}$ globally (with an average difference of ~15%), although contributions of ψ_L are nontrivial and likely underestimated because of the difficulty of estimating ψ_L (further discussed below). The probability density function of the Pearson correlation coefficient between the resulting $VOD_{est.}$ and VOD is shown in Figure 5. The 8 day averaged VOD, LAI, and soil moisture data during 2003–2010 with 0.25° resolutions are used to create this figure. About 64% of the pixels have $R(\text{VOD}, \text{VOD}_{est.}) > 0.6$, indicating the general suitability of this approach for studying the relative contributions of ψ_L and LAI to X-band VOD despite the number of significant assumptions involved. The partial correlations of VOD with $\psi_L^{est.}$ and LAI are also shown in Figure 5 (defined in section 2.2.2). Although the influence of both $\psi_L^{est.}$ and LAI on VOD is expected to be positive, 11% of the values of the partial correlation with VOD and $\psi_L^{est.}$ (conditioned on LAI) and 12% of the values of the partial correlation between VOD and LAI (conditioned on $\psi_L^{est.}$) are negative. This is likely due to errors in the assumptions relating remotely sensed surface soil moisture to ψ_L. Because the quality of the estimation of $\psi_L^{est.}$ from surface soil moisture (sm) is uncertain, we performed a sensitivity analysis using soil moisture directly instead of ψ_s. The performance of the conceptual model was qualitatively similar, although the median of R(VOD, sm:LAI) and R(VOD, LAI:sm) decreased by 3% and 6%, respectively, compared to $R(\text{VOD}, \psi_L^{est.}\text{:LAI})$ and $R(\text{VOD}, \text{LAI}:\psi_L^{est.})$ and the corresponding peaks of the probability density functions decreased by 15% and 5%, respectively (Figure S2). Hence, despite the uncertainty inherent in the soil texture data and pedotransfer functions used, accounting for the nonlinearity and spatial variability of the relationship between sm and ψ_s by explicitly estimating ψ_s increases the partial correlations of LAI and ψ_s with VOD.

The coefficient of determination of the regression between the observed VOD and $VOD_{est.}$ across the globe is shown in Figure 6a. Despite the large number of assumptions necessary to estimate ψ_L at a global scale, the reconstruction captures about 70% of the variability of the observed VOD in much of Europe, India, the Southeastern United States, the Sahel, and African woodlands. The partial correlations allow us to investigate the relative contribution of LAI and ψ_s in the VOD signal (Figure S3). The correlation map between VOD and LAI is qualitatively similar to correlation coefficient map between VOD and NDVI plotted in Liu, De Jeu, et al. (2011).

The correlation of VOD with $VOD_{est.}$ obtained from the full conceptual model is higher than the partial correlations of VOD with ψ_L^{est} and LAI. The relative contributions of $\psi_L^{est.}$ and LAI are shown in Figures 6b and 6c. The difference between the correlation coefficient of the full conceptual model and the partial correlation coefficient with LAI accounting for $\psi_L^{est.}$ shows the added information content obtained by accounting for the effect of water stress on both time-varying and time-invariant AGB components. Similarly, the difference between the correlation coefficient of the full conceptual model and the partial correlation coefficient with $\psi_L^{est.}$ accounting for LAI shows the effect of accounting for biomass in deriving water stress information from VOD. The $VOD_{est.}$ derived from the full conceptual model improves the partial correlation of VOD with $\psi_L^{est.}$ by about 31% on average and the partial correlation of VOD with LAI by about 15%. The effect of water stress on VOD is most significant in several dry regions (e.g., central Australia, the western United States, and vegetated parts of the Middle East), but Figure 6c also shows high values in several wetter regions, including Northeastern Brazil, Northern India, and Southern Russia. We note that because the errors associated with estimating ψ_L from remotely sensed soil moisture are likely significantly larger than the errors in LAI retrievals, Figure 6c is likely an underestimate of the contribution of ψ_L to VOD. Hence, the variability of both AGB and RWC should be considered when investigating the temporal dynamics of VOD signal.

To further understand these spatial patterns, we examined the correlation components as a function of mean pixel VOD (Figure 7). The partial correlation of VOD with $\psi_L^{est.}$ decreases as mean VOD increases (Figure 7a) whereas the partial correlation of VOD with LAI increases as mean VOD increases (Figure 7b). Thus, the dynamics of VOD are more correlated with LAI when mean VOD is high and is more correlated with $\psi_L^{est.}$ when mean VOD is low. The mean pixel VOD is well correlated with mean precipitation, LAI, and canopy

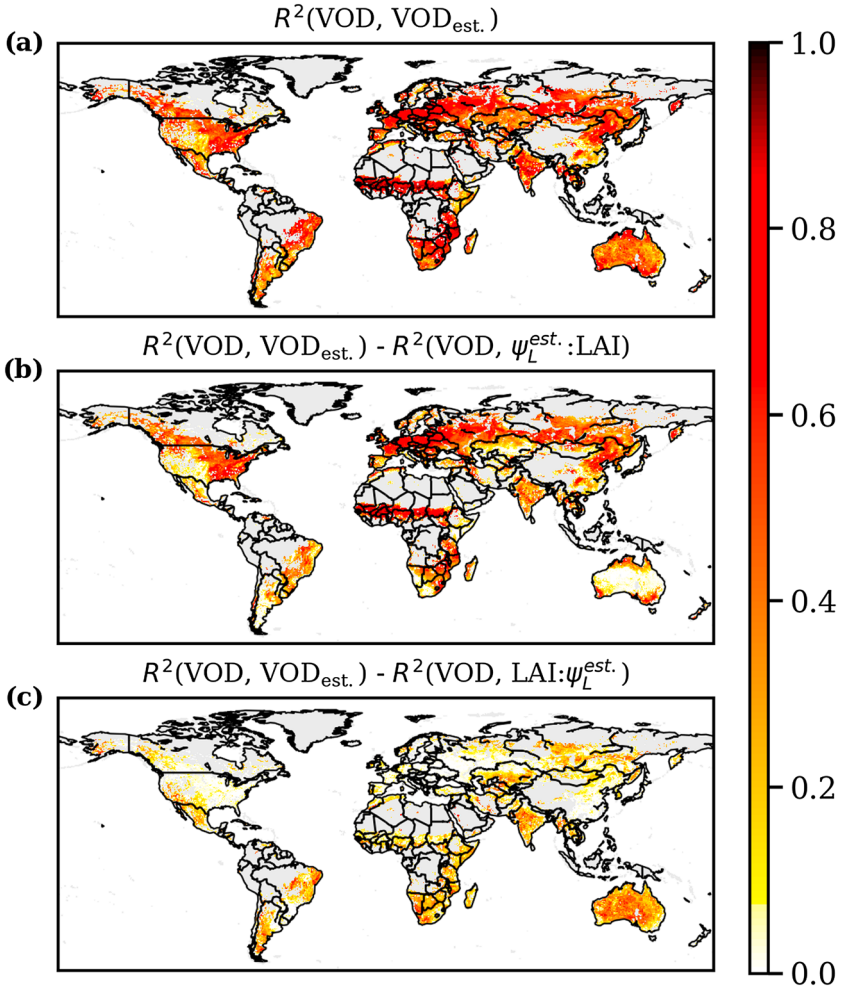

Figure 6. (a) Explained variability in VOD by using a constrained multiple linear regression of the conceptual model (VOD$_{est.}$); (b) global difference map between the coefficient of determination of the full conceptual model (accounting for both LAI and $\psi_L^{est.}$ terms) and the square of the partial correlation of VOD with $\psi_L^{est.}$ accounting for the effect of LAI, showing the contributions of biomass-driven terms to VOD$_{est.}$; and (c) global difference map between the coefficient of determination of the full conceptual model (accounting for both LAI and $\psi_L^{est.}$ terms) and the square of the partial correlation of VOD with LAI accounting for the effect of $\psi_L^{est.}$, showing the contributions of $\psi_L^{est.}$-driven terms to VOD$_{est.}$. Pixels, which are covered by tropical forests, have annual average LAI < 0.05, or contain less than 75% of possible data points (either due to a lack of overpasses or filtering of rainy days), were removed from the analysis, and are shown with a gray mask.

height (Figure S4). This implies that in drier regions with sparse vegetation covers, VOD is more correlated with plant water stress while in wetter regions with denser and taller canopy heights VOD is more correlated with LAI. However, neither the partial nor the full correlation distributions change significantly across land cover types (Figure S5, except perhaps slightly higher $\psi_L^{est.}$ partial correlations for nonwoody cover types), suggesting that this effect is due to vegetation density itself and not differences in canopy structure. Unlike the partial correlations, the overall ability of the conceptual model to explain the variability of VOD is independent of mean VOD (Figure 7c) as it combines the opposite trends of partial correlations and outperforms both of them across different land-cover types (Figure S5).

As discussed in section 3, the regression intercept in equation (5) is expected to be proportional to the amount of dry AGB in the static biomass components, for example, stems and branches. We therefore expected it to increase with average canopy height. The scatterplot in Figure 8a shows the correlations between these two quantities with $R^2 = 0.6$ for all data points. Figure 8b depicts the variability of the intercept across different land-cover types. As expected, the intercept values are higher for woody, forested land cover types with large stems than for nonwoody types like grasslands, croplands, and savannas. Similarly, the estimated intercepts are generally slightly higher in woody savannas than in savannas.

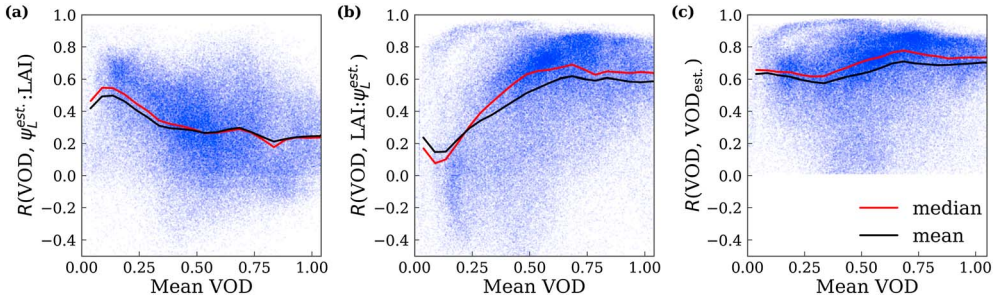

Figure 7. Dependence of the partial correlations and full-term correlation on mean VOD. Scatterplots of correlations against mean VOD: (a) the partial correlation of VOD with LAI accounting for the effect of $\psi_L^{est.}$, (b) the partial correlation of VOD with $\psi_L^{est.}$ accounting for the effect of LAI, and (c) the correlation of the suggested full-term equation against mean VOD signal. The mean is shown as a black line, while the median is shown in red.

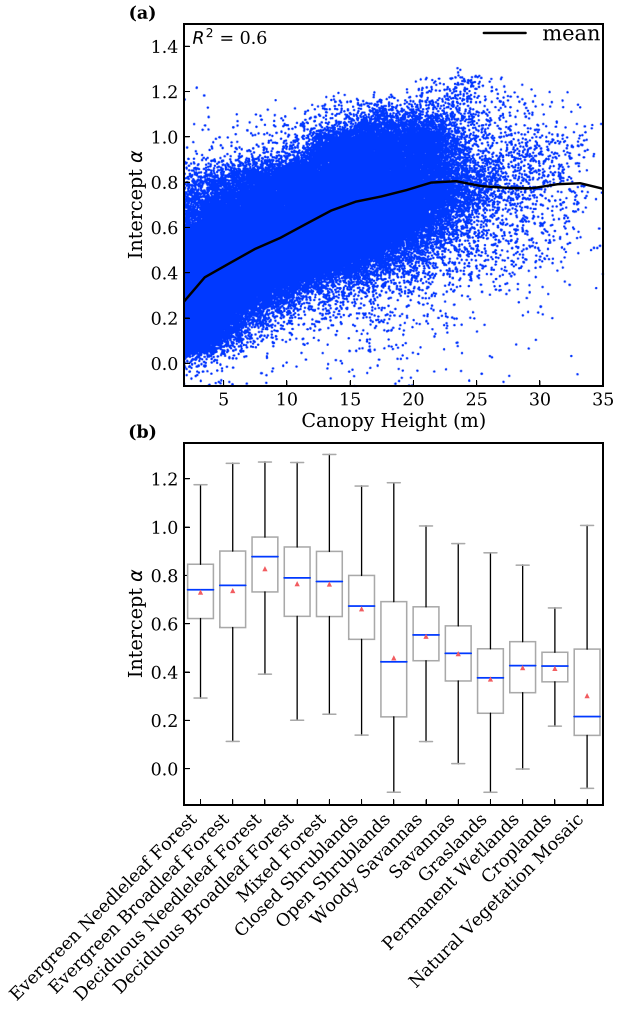

Figure 8. Regression intercept variability with canopy properties: (a) relationship between canopy height and the intercept of the full-term equation, α, and (b) the distribution of α across different land-cover types. Note that we removed pixels that contained significant urban and built-up land cover category due to contamination of VOD signal in such regions.

4. Discussion

At the three sites studied in this paper, the comparison of VOD to ψ_L observations showed a dominant role of water stress compared to phenological changes, although the effect of phenology may be underestimated at deciduous MOFLUX and Morgan–Monroe sites—where measurements of ψ_L were generally not available during the start and end of the growing season when LAI is changing most rapidly. At the global scale, LAI changes were more significant, contributing on average almost twice as much to the total correlation between VOD and the optimally explained VOD as $\psi_L^{est.}$ did. However, because the estimates of ψ_L at global scales are significantly more error-prone than the remote sensing estimates of LAI, the global-scale analyses likely underestimate the effect of ψ_L on VOD. Taken together, neither the role of phenology nor the role of water stress can be neglected in studying VOD dynamics.

The electromagnetic sensitivity of VOD to different canopy components is known to vary based on both land cover type and electromagnetic frequency (Ulaby & Long, 2014), complicating the interpretation of VOD dynamics. We focused on the X-Band (~10 GHz) frequency VOD data set here due to its longer record through the AMSR-E and AMSR2 satellite observations and since high frequency data are likely relatively more sensitive to leaves rather than heterogeneous understory cover or stems. Carrying out the same global analysis using lower-frequency C-band (~6.5 GHz) VOD indicated that the correlations of our full-term equation with C-Band VOD retrievals decreased about 5% on average compared to the X-band VOD retrievals (Figure S6).

Although not tested here because they cover significantly different time periods, lower L-band (~1.2 GHz) VOD records may be more sensitive to stems and other woody components, which contain a majority of total plant water in most species (Hornbuckle & England, 2004; Sternberg & Shoshany, 2000). Thus, L-band records such as those from SMOS (Fernandez-Moran et al., 2017) or SMAP (Konings, Piles, et al., 2017) may be particularly useful for studies investigating the role of changes in woody tissue water storage (e.g., Köcher et al., 2013) or studies of woody encroachment (Brandt et al., 2017; Tian et al., 2017).

Even at the X-band frequency studied here, errors in the retrieval of VOD from the observed brightness temperatures may also influence the interpretation of its sensitivity. The analyses were repeated for

VOD retrieved from the same sensors using an alternative algorithm, the Land Parameter Data Record (Du et al., 2017) with different estimation techniques for (among others) the effects of land surface temperature, scattering albedo, and contributions from open water bodies. The site-level validations did not change significantly. Similarly, the global average sensitivity to LAI and ψ_L were similar. In most areas, the total correlation between VOD and $VOD_{est.}$ differed by less than ~10% between the two algorithms. However, large differences of more than 30% occurred in several high-latitude regions with numerous open water bodies (where the Land Parameter Data Record retrievals performed better) and in densely forested sites in the Southeastern US and Southeastern China (where the LPRM retrievals performed better; see Figure S7).

While the focus of this paper was to explore the sensitivities of passive microwave-based VOD data, active microwave (e.g., radar) observations are also sensitive to water content and may therefore exhibit some of the same sensitivities exhibited here. Indeed, several studies have recently interpreted diurnal (Friesen et al., 2012; Frolking et al., 2011; Konings, Yu, et al., 2017; Steele-dunne et al., 2012; van Emmerik et al., 2015) and seasonal (Saatchi et al., 2013; van Emmerik et al., 2017) dynamics of backscattering coefficients as sensitive to water stress. For instance, van Emmerik et al. (2017) showed that Ku-band radar backscattering coefficients observed by RapidScat follow the dynamics of stem water content measured by dendrometers in the Amazon.

Nevertheless, both the local and global scale analyses performed in this study are potentially sensitive to a range of error sources, including errors from hysteresis or nonlinearity in the VWC–ψ_L relationship, errors in the LAI data sets, or effects of phenologically varying biomass components not captured by LAI (e.g., fruit and wet litter). The global analyses neglect the role of growth of woody components and possible disturbance (e.g., harvesting and fire) across the 8 years of the AMSR-E record studied and may thus underestimate the effect of biomass changes on the overall VOD dynamics. Taken together with the errors in the $\psi_L^{est.}$ that suggested the contribution of ψ_L is also underestimated may explain why, for most pixels, only about 70% of the overall VOD dynamics are accounted for by the new conceptual model.

The site-level comparisons were sensitive to the effects of subpixel heterogeneity and differences in between the time of day at which ψ_L measurements were collected and the 1:30 AM/PM overpass times of the satellites. By contrast, the global-scale estimation was most sensitive to errors in the estimation of ψ_L from remotely sensed surface soil moisture including difference between surface soil and root-zone soil moisture estimates, errors in soils or pedotransfer data used to relate soil moisture to ψ_s, and incomplete equilibration between ψ_s and ψ_L for at least some of the species at the 1:30 AM overpass time of the VOD measurements. Furthermore, possible seasonal biases introduced by filtering rainy days, particularly in areas with a strong rainy season, can lead to errors. However, since filtering the rainy days improves the averaged correlations by only up to 4% globally compared to the nonfiltered data and spatial patterns in the different correlations do not change significantly, this effect may be minor. Overall, the conceptual model accounting for both water stress through changes in ψ_L and phenological changes is able to explain a majority of the observed VOD dynamics.

The sensitivity of VOD to ψ_L demonstrated here underscores the potential utility of VOD in plant hydraulic studies. At this time, it is not possible to predict a priori the coefficients in the conceptual model relating VOD to ψ_L and LAI. Although these coefficients are time-invariant, the high expected error in the estimates of global ψ_L likely affects the absolute values of the regression parameters. This prevents a direct determination of ψ_L from VOD. Additional radiative transfer or plant physiological studies may continue to provide insight into optimal parameter values, although we are not presently aware of any site where repeated measurements of both biomass and leaf water potential are available. In the meantime, VOD observations may prove particularly useful in studies where regression parameters can be explicitly retrieved or in quantitative studies where an exact parameterization of the VOD–ψ_L relationship is not necessary, for example, statistical (or machine learning-based) predictions. Observations from optical remote sensing (such as LAI), soil moisture, or gravitational data reflecting total columnar water content may all be useful inputs in such statistical models. Regardless of the methodology or training data sets, additional research is required to robustly account for the effect of biomass dynamics on VOD in order to determine water potential and vice versa.

5. Conclusions

In this paper, we introduced a conceptual framework for analyzing variations in microwave VOD—proportional to vegetation water content—in terms of both changes in leaf area index and leaf water potential, ψ_L. Observed X-band VOD signals from AMSR-E were estimated from four terms incorporating the effects of total canopy biomass, ψ_L, and their interactions. The validity of the conceptual model was examined using ψ_L observations at three field sites in the United States—an evergreen woodland at Sevilleta, NM and two deciduous forests in Missouri and Indiana. The estimated VOD matched the true observed VOD signal, with high coefficients of determination for each of the three studied sites (R^2 = 0.64–0.8).

To increase the variety of ecosystems for which VOD sensitivities could be analyzed, ψ_L values were estimated at a global scale with the help of surface soil water potential data, assuming predawn equilibrium. The final estimated VOD signal improves the partial correlation of true VOD with $\psi_L^{est.}$ ~30% on average and the partial correlation of VOD with LAI ~15%, indicating sensitivity to both phenology and water stress. In wetter regions with denser and taller canopy heights (higher mean VOD), VOD was more highly correlated with LAI than water potential. By contrast, in drier regions with sparser vegetation covers, VOD had higher correlations with plant water potential.

Our simplified conceptual framework enables better understanding of the contributions of phenology and water stress to VOD dynamics. Because both LAI and ψ_L affect VOD, trends in VOD at a given location are sensitive to both factors. Therefore, care must be taken that interpretations of VOD trends as biomass trends also account for the hydrological effects (e.g., water stress related) on VOD. The sensitivity of VOD dynamics to ψ_L (along with biomass dynamics) demonstrated here suggests the potential utility of remotely sensed VOD data sets in studies of ecohydrological processes in plants and vegetated landscapes.

Acknowledgments

The LAI data product was retrieved from the online Data Pool, courtesy of the NASA Land Processes Distributed Active Archive Center (LP DAAC), USGS/Earth Resources Observation and Science (EROS) Center, Sioux Falls, South Dakota, https://lpdaac.usgs.gov/data_access/data_pool. The authors acknowledge support from the US Department of Energy via the AmeriFlux Management Project for continued operations of the Morgan–Monroe State Forest AmeriFlux site. US DOE supported the Sevilleta study, and Lab Directed Research and Development at Pacific Northwest National Laboratory supported N.M. AmeriFlux site US-MOz and J.D.W. are supported by the U.S. Department of Energy, Office of Science, Office of Biological and Environmental Research Program, through Oak Ridge National Laboratory's Terrestrial Ecosystem Science (TES) Science Focus Area (SFA). ORNL is managed by UT-Battelle, LLC, for the U.S. DOE under contract DE-AC05-00OR22725.

References

Andela, N., Liu, Y. Y., Van Dijk, A. I. J. M., De Jeu, R. A. M., & McVicar, T. R. (2013). Global changes in dryland vegetation dynamics (1988–2008) assessed by satellite remote sensing: Comparing a new passive microwave vegetation density record with reflective greenness data. *Biogeosciences*, *10*(10), 6657–6676. https://doi.org/10.5194/bg-10-6657-2013

Bartlett, M. K., Scoffoni, C., & Sack, L. (2012). The determinants of leaf turgor loss point and prediction of drought tolerance of species and biomes: A global meta-analysis. *Ecology Letters*, *15*(5), 393–405. https://doi.org/10.1111/j.1461-0248.2012.01751.x

Bonan, G. B., Williams, M., Fisher, R. A., & Oleson, K. W. (2014). Modeling stomatal conductance in the earth system: Linking leaf water-use efficiency and water transport along the soil–plant–atmosphere continuum. *Geoscientific Model Development*, *7*(5), 2193–2222. https://doi.org/10.5194/gmd-7-2193-2014

Boyer, J. S. (1967). Plant–water relationships. *Science*, *158*(3805), 1171 LP-1172.

Brandt, M., Rasmussen, K., Peñuelas, J., Tian, F., Schurgers, G., Verger, A., … Fensholt, R. (2017). Human population growth offsets climate-driven increase in woody vegetation in sub-Saharan Africa. *Nature Ecology and Evolution*, *1*(4), 4–9. https://doi.org/10.1038/s41559-017-0081

Brooks, R. H., & Corey, A. T. (1964). *Hydraulic properties of porous media*, *Hydrology paper* (Vol. 3, p. 27). Fort Collins, CO: Colorado State University.

Christoffersen, B. O., Gloor, M., Fauset, S., Fyllas, N. M., Galbraith, D. R., Baker, T. R., … Rowland, L. (2016). Linking hydraulic traits to tropical forest function in a size-structured and trait-driven model (TFS v. 1-Hydro). *Geoscientific Model Development*, *9*(11), 4227–4255. https://doi.org/10.5194/gmd-9-4227-2016.

Donovan, L. A., Richards, J. H., & Linton, M. J. (2003). Magnitude and mechanisms of disequilibrium between predawn plant and soil water potentials. *Ecology*, *84*(2), 463–470. https://doi.org/10.1890/0012-9658(2003)084%5B0463:MAMODB%5D2.0.CO;2

Du, J., Kimball, J. S., Jones, L. A., Kim, Y., Glassy, J., & Watts, J. D. (2017). A global satellite environmental data record derived from AMSR-E and AMSR2 microwave Earth observations. *Earth System Science Data Discussions*, *9*(2), 791–808. https://doi.org/10.5194/essd-9-791-2017

Du, J., Kimball, J. S., Shi, J., Jones, L. A., Wu, S., Sun, R., & Yang, H. (2014). Inter-calibration of satellite passive microwave land observations from AMSR-E and AMSR2 using overlapping FY3B-MWRI sensor measurements. *Remote Sensing*, *6*(9), 8594–8616. https://doi.org/10.3390/rs6098594

Fernandez-Moran, R., Al-Yaari, A., Mialon, A., Mahmoodi, A., Al Bitar, A., De Lannoy, G., … Wigneron, J.-P. (2017). SMOS-IC: An alternative SMOS soil moisture and vegetation optical depth product. *Remote Sensing*, *9*(5), 457. https://doi.org/10.3390/rs9050457

Fischer, G., Nachtergaele, F. O., Prieler, S., Teixeira, E., Géza, T., Van Velthuizen, H., Verelst, L., & Wiberg, D. (2010). Global Agro-Ecological Zones(GAEZ v3.0)—model documentation, IIASA, Laxenburg, Austria and FAO, Rome, Italy.

Forkel, M., Dorigo, W., Lasslop, G., Teubner, I., Chuvieco, E., & Thonicke, K. (2016). Identifying required model structures to predict global fire activity from satellite and climate data. *Geoscientific Model Development Discussion*, 1–35. https://doi.org/10.5194/gmd-2016-301

Friedl, M. A., Sulla-menashe, D., Tan, B., Schneider, A., Ramankutty, N., Sibley, A., & Huang, X. (2010). Remote sensing of environment MODIS collection 5 global land cover: Algorithm refinements and characterization of new datasets. *Remote Sensing of Environment*, *114*(1), 168–182. https://doi.org/10.1016/j.rse.2009.08.016

Friesen, J., Steele-dunne, S. C., & Van De Giesen, N. (2012). Diurnal differences in global ERS scatterometer backscatter observations of the land surface. *IEEE Transactions on Geoscience and Remote Sensing*, *50*(7), 2595–2602. https://doi.org/10.1109/TGRS.2012.2193889

Frolking, S., Milliman, T., Palace, M., Wisser, D., Lammers, R., & Fahnestock, M. (2011). Tropical forest backscatter anomaly evident in SeaWinds scatterometer morning overpass data during 2005 drought in Amazonia. *Remote Sensing of Environment*, *115*(3), 897–907. https://doi.org/10.1016/j.rse.2010.11.017

Gentine, P., Guerin, M., Uriarte, M., Mcdowell, N. G., & Pockman, W. T. (2015). An allometry-based model of the survival strategies of hydraulic failure and carbon starvation. *Ecohydrology*, *9*(3), 529–546. https://doi.org/10.1002/eco.1654

Gu, L., Pallardy, S. G., Hosman, K. P., & Sun, Y. (2015). Drought-influenced mortality of tree species with different predawn leaf water dynamics in a decade-long study of a central US forest. *Biogeosciences*, *12*(10), 2831–2845. https://doi.org/10.5194/bg-12-2831-2015

Gu, L., Pallardy, S. G., Yang, B., Hosman, K. P., Mao, J., Ricciuto, D., … Sun, Y. (2016). Testing a land model in ecosystem functional space via a comparison of observed and modeled ecosystem flux responses to precipitation regimes and associated stresses in a Central U.S. forest. *Journal of Geophysical Research: Biogeosciences*, *121*(7), 1884–1902. https://doi.org/10.1002/2015JG003302

Guan, K., Wood, E. F., Medvigy, D., Kimball, J., Pan, M., Caylor, K. K., … Jones, M. O. (2014). Terrestrial hydrological controls on land surface phenology of African savannas and woodlands Kaiyu. *Journal of Geophysical Research: Biogeosciences*, *119*, 1652–1669. https://doi.org/10.1002/2013JG002572

Guglielmetti, M., Schwank, M., Mätzler, C., Oberdörster, C., Vanderborght, J., & Flühler, H. (2007). Measured microwave radiative transfer properties of a deciduous forest canopy. *Remote Sensing of Environment*, *109*(4), 523–532. https://doi.org/10.1016/j.rse.2007.02.003

Herrera, A., Ballestrini, C., & Tezara, W. (2008). Nocturnal sap flow in the C3-CAM species, Clusia minor. *Trees*, *22*(4), 491–497. https://doi.org/10.1007/s00468-008-0209-8

Hornbuckle, B. K., & England, A. W. (2004). Radiometric sensitivity to soil moisture at 1.4 GHz through a corn crop at maximum biomass. *Water Resources Research*, *40*, W10204. https://doi.org/10.1029/2003WR002931

Hornbuckle, B. K., Patton, J. C., Vanloocke, A., Suyker, A. E., Roby, M. C., Walker, V. A., … Endacott, E. A. (2016). SMOS optical thickness changes in response to the growth and development of crops, crop management, and weather. *Remote Sensing of Environment*, *180*, 320–333. https://doi.org/10.1016/j.rse.2016.02.043

Huffman, G. J., Adler, R. F., Bolvin, D. T., Gu, G., Nelkin, E. J., Bowman, K. P., … Wolff, D. B. (2007). The TRMM multisatellite precipitation analysis (TMPA): Quasi-global, multiyear, combined-sensor precipitation estimates at fine scales. *Journal of Hydrometeorology*, *8*(1), 38–55. https://doi.org/10.1175/JHM560.1

Jackson, T. J., & Schmugge, T. J. (1991). Vegetation effects on the microwave emission of soils. *Remote Sensing of Environment*, *36*(3), 203–212. https://doi.org/10.1016/0034-4257(91)90057-D

Jarvis, P. G. (1976). The interpretation of the variations in leaf water potential and stomatal conductance found in canopies in the field. *Philosophical Transactions of the Royal Society of London*, *273*(927), 593–610. https://doi.org/10.1098/rstb.1976.0035

Jones, M. O., Jones, L. A., Kimball, J. S., & McDonald, K. C. (2011). Satellite passive microwave remote sensing for monitoring global land surface phenology. *Remote Sensing of Environment*, *115*(4), 1102–1114. https://doi.org/10.1016/j.rse.2010.12.015

Jones, M. O., Kimball, J. S., & Jones, L. A. (2013). Satellite microwave detection of boreal forest recovery from the extreme 2004 wildfires in Alaska and Canada. *Global Change Biology*, *19*(10), 3111–3122. https://doi.org/10.1111/gcb.12288

Jones, M. O., Kimball, J. S., Jones, L. A., & McDonald, K. C. (2012). Satellite passive microwave detection of North America start of season. *Remote Sensing of Environment*, *123*, 324–333. https://doi.org/10.1016/j.rse.2012.03.025

Jones, H. G., & Vaughan, R. (2010). *Remote sensing of vegetation: Principles, techniques, and applications*. Oxford: Oxford University Press.

Köcher, P., Horna, V., & Leuschner, C. (2013). Stem water storage in five coexisting temperate broad-leaved tree species: Significance, temporal dynamics and dependence on tree functional traits. *Tree Physiology*, *33*(8), 817–832. https://doi.org/10.1093/treephys/tpt055

Konings, A. G., & Gentine, P. (2017). Global variations in ecosystem-scale isohydricity. *Global Change Biology*, *23*, 891–905. https://doi.org/10.1111/gcb.13389

Konings, A. G., Piles, M., Das, N., & Entekhabi, D. (2017). Remote sensing of environment L-band vegetation optical depth and effective scattering albedo estimation from SMAP. *Remote Sensing of Environment*, *198*, 460–470. https://doi.org/10.1016/j.rse.2017.06.037

Konings, A. G., Piles, M., Rötzer, K., McColl, K. A., Chan, S. K., & Entekhabi, D. (2016). Vegetation optical depth and scattering albedo retrieval using time series of dual-polarized L-band radiometer observations. *Remote Sensing of Environment*, *172*, 178–189. https://doi.org/10.1016/j.rse.2015.11.009

Konings, A. G., Williams, A. P., & Gentine, P. (2017). Sensitivity of grassland productivity to aridity controlled by stomatal and xylem regulation. *Nature Geoscience*, *10*(4), 284–288. https://doi.org/10.1038/NGEO2903

Konings, A. G., Yu, Y., Xu, L., Yang, Y., Schimel, D. S., & Saatchi, S. S. (2017). Active microwave observations of diurnal and seasonal variations of canopy water content across the humid African tropical forests. *Geophysical Research Letters*, *44*, 2290–2299. https://doi.org/10.1002/2016GL072388

Larcher, W. (1995). *Physiological plant ecology*. Berlin, Germany: Springer. https://doi.org/10.1007/978-3-642-87851-0

Lawrence, H., Wigneron, J.-P., Richaume, P., Novello, N., Grant, J., Mialon, A., … Merlin, O. (2014). Comparison between SMOS vegetation optical depth products and MODIS vegetation indices over crop zones of the USA. *Remote Sensing of Environment*, *140*, 396–406. https://doi.org/10.1016/j.rse.2013.07.021

Liang, S., & Xiao, Z. (2012). *Global land surface products: Leaf area index product data collection (1985–2010)*. Beijing: Beijing Normal University https://doi.org/10.6050/glass863.3004.db

Liu, Y. Y., De Jeu, R. A. M., McCabe, M. F., Evans, J. P., & Van Dijk, A. I. J. M. (2011). Global long-term passive microwave satellite-based retrievals of vegetation optical depth. *Geophysical Research Letters*, *38*, L18402. https://doi.org/10.1029/2011GL048684

Liu, Y. Y., Dorigo, W. A., Parinussa, R. M., De Jeu, R. A. M., Wagner, W., McCabe, M. F., … Van Dijk, A. I. J. M. (2012). Trend-preserving blending of passive and active microwave soil moisture retrievals. *Remote Sensing of Environment*, *123*, 280–297. https://doi.org/10.1016/j.rse.2012.03.014

Liu, Y. Y., Evans, J. P., McCabe, M. F., de Jeu, R. A. M., van Dijk, A. I. J. M., Dolman, A. J., & Saizen, I. (2013). Changing climate and overgrazing are decimating Mongolian steppes. *PLoS One*, *8*(2), e57599–e57599. https://doi.org/10.1371/journal.pone.0057599

Liu, Y. Y., Parinussa, R. M., Dorigo, W. A., De Jeu, R. A. M., Wagner, W., Van Dijk, A. I. J. M., & Mccabe, M. F. (2011). Developing an improved soil moisture dataset by blending passive and active microwave satellite-based retrievals, *15*, 425–436. https://doi.org/10.5194/hess-15-425-2011

Liu, Y. Y., van Dijk, A. I. J. M., de Jeu, R. A. M., Canadell, J. G., McCabe, M. F., Evans, J. P., & Wang, G. (2015). Recent reversal in loss of global terrestrial biomass. *Nature Climate Change*, *5*(5), 470–474. https://doi.org/10.1038/nclimate2581

Manzoni, S., Katul, G., & Porporato, A. (2014). Optimal plant water-use strategies under stochastic rainfall. *Water Resources Research*, *50*, 5170–5183. https://doi.org/10.1002/2013WR015236

Matheny, A. M., Mirfenderesgi, G., & Bohrer, G. (2017). Trait-based representation of hydrological functional properties of plants in weather and ecosystem models. *Plant Diversity*, *39*(1), 1–12. https://doi.org/10.1016/j.pld.2016.10.001

Meesters, A. G. C. A., De Jeu, R. A. M., & Owe, M. (2005). Analytical derivation of the vegetation optical depth from the microwave polarization difference index. *IEEE Geoscience and Remote Sensing Letters*, *2*(2), 121–123. https://doi.org/10.1109/LGRS.2005.843983

Momen, M., & Bou-Zeid, E. (2016). Large Eddy simulations and damped-oscillator models of the unsteady Ekman boundary layer. *Journal of the Atmospheric Sciences*, *73*(1), 25–40. https://doi.org/10.1175/JAS-D-15-0038.1

Momen, M., & Bou-Zeid, E. (2017). Analytical reduced models for non-stationary diabatic atmospheric boundary layers. *Boundary-Layer Meteorology*, *164*(3), 383–399. https://doi.org/10.1007/s10546-017-0247-0

Morton, D. C., Nagol, J., Carabajal, C. C., Rosette, J., Palace, M., Cook, B. D., … North, P. R. J. (2014). Amazon forests maintain consistent canopy structure and greenness during the dry season. *Nature*, *506*(7487), 221–224. https://doi.org/10.1038/nature13006

Owe, M., de Jeu, R., & Holmes, T. (2008). Multisensor historical climatology of satellite-derived global land surface moisture. *Journal of Geophysical Research*, *113*, F01002. https://doi.org/10.1029/2007JF000769

Parinussa, R. M., Holmes, T. R. H., Wanders, N., Dorigo, W. A., & De Jeu, R. A. M. (2015). A preliminary study toward consistent soil moisture from AMSR2. *Journal of Hydrometeorology*, *16*(2), 932–947. https://doi.org/10.1175/JHM-D-13-0200.1

Pearcy, R. W., Ehleringer, J., Mooney, H. A., & Rundel, P. W. (Eds.) (1989). *Plant physiological ecology: Field methods and instrumentation*. London: Chapman & Hall. https://doi.org/10.1007/978-94-009-2221-1

Phillips, N. G., Ryan, M. G., Bond, B. J., Dowell, N. G. M. C., Hinckley, T. M., & Ermák, J. È. (2003). Reliance on stored water increases with tree size in three species in the Pacific Northwest. *Tree Physiology*, *23*(4), 237–245. https://doi.org/10.1093/treephys/23.4.237

Plaut, J. A., Yepez, E. A., Hill, J., Pangle, R., Sperry, J. S., Pockman, W. T., & Mcdowell, N. G. (2012). Hydraulic limits preceding mortality in a piñon–juniper woodland under experimental drought. *Plant, Cell and Environment*, *35*(9), 1601–1617. https://doi.org/10.1111/j.1365-3040.2012.02512.x

Roman, D. T., Novick, K. A., Brzostek, E. R., Dragoni, D., Rahman, F., & Phillips, R. P. (2015). The role of isohydric and anisohydric species in determining ecosystem-scale response to severe drought. *Oecologia*, *179*(3), 641–654. https://doi.org/10.1007/s00442-015-3380-9

Saatchi, S., Ase, S., Malhi, Y., Aragão, L. E. O. C., & Anderson, L. O. (2013). Persistent effects of a severe drought on Amazonian forest canopy. *Proceedings of the National Academy of Sciences*, *110*(2), 565–570. https://doi.org/10.1073/pnas.1204651110

Saleh, K., Wigneron, J. P., De Rosnay, P., Calvet, J. C., Escorihuela, M. J., Kerr, Y., & Waldteufel, P. (2006). Impact of rain interception by vegetation and mulch on the L-band emission of natural grass. *Remote Sensing of Environment*, *101*(1), 127–139. https://doi.org/10.1016/j.rse.2005.12.004

Santi, E., Paloscia, S., Pampaloni, P., & Pettinato, S. (2009). Ground-based microwave investigations of forest plots in Italy. *IEEE Transactions on Geoscience and Remote Sensing*, *47*(9), 3016–3025. https://doi.org/10.1109/TGRS.2009.2021613

Schmid, H. P., Grimmond, C. S. B., Cropley, F., Offerle, B., & Su, H. B. (2000). Measurements of CO_2 and energy fluxes over a mixed hardwood forest in the mid-western United States. *Agricultural and Forest Meteorology*, *103*(4), 357–374. https://doi.org/10.1016/S0168-1923(00)00140-4

Simard, M., Pinto, N., Fisher, J. B., & Baccini, A. (2011). Mapping forest canopy height globally with spaceborne lidar. *Journal of Geophysical Research*, *116*, G04021. https://doi.org/10.1029/2011JG001708

Sperry, J. S., & Tyree, M. T. (1988). Mechanism of water stress-induced xylem embolism. *Plant Physiology*, *88*(3), 581–587. https://doi.org/10.1104/pp.88.3.581

Steele-dunne, S. C., Friesen, J., & Van De Giesen, N. (2012). Using diurnal variation in backscatter to detect vegetation water stress. *IEEE Transactions on Geoscience and Remote Sensing*, *50*(7), 2618–2629. https://doi.org/10.1109/TGRS.2012.2194156

Sternberg, M., & Shoshany, M. (2000). Aboveground biomass allocation and water content relationships in Mediterranean trees and shrubs in two climatological regions in Israel. *Plant Ecology*, *157*(2), 173–181.

Tian, F., Brandt, M., Liu, Y. Y., Rasmussen, K., & Fensholt, R. (2017). Mapping gains and losses in woody vegetation across global tropical drylands. *Global Change Biology*, *23*(4), 1748–1760. https://doi.org/10.1111/gcb.13464

Tian, F., Brandt, M., Liu, Y. Y., Verger, A., Tagesson, T., Diouf, A. A., … Fensholt, R. (2016). Remote sensing of vegetation dynamics in drylands: Evaluating vegetation optical depth (VOD) using AVHRR NDVI and in situ green biomass data over west African Sahel. *Remote Sensing of Environment*, *177*, 265–276. https://doi.org/10.1016/j.rse.2016.02.056

Ulaby, F. T., & Long, D. G. (2014). *Microwave radar and radiometric remote sensing*. Ann Arbon, MI: University of Michigan Press. https://doi.org/10.3998/0472119356

Ulaby, F. T., Moore, R., & Fung, A. (1982). *Microwave remote sensing: Active and passive* (2nd ed.). Reading, MA: Addison-Wesley.

van Emmerik, T., Member, S., Steele-dunne, S. C., Judge, J., Member, S., & Van De Giesen, N. (2015). Impact of diurnal variation in vegetation water content on radar backscatter from maize during water stress. *IEEE Geoscience and Remote Sensing Letters*, *53*(7), 3855–3869. https://doi.org/10.1109/TGRS.2014.2386142

van Emmerik, T., Steele-Dunne, S. C., Judge, J., & van de Giesen, N. (2017). Dielectric response of corn leaves to water stress. *IEEE Geoscience and Remote Sensing Letters*, *14*(1), 8–12. https://doi.org/10.1109/LGRS.2016.2606662

Wagner, W., Dorigo, W., de Jeu, R., Fernandez, D., Benveniste, J., Haas, E., & Ertl, M. (2012). Fusion of active and passive microwave observations to create an essential climate variable data record on soil moisture. *Remote Sensing and Spatial Information Sciences*, *1-7*, 315–321.

Wieder, W. R., Boehnert, J., Bonan, G. B., & Langseth, M. (2012). Regridded harmonized world soil database v1.2. Data set. Oak Ridge, TN: Oak Ridge National Laboratory Distributed Active Archive Center. Retrieved from http://daac.ornl.gov. https://doi.org/10.3334/ORNLDAAC/1247

Wigneron, J.-P., Pardé, M., Waldteufel, P., Chaqzy, A., Kerr, Y., Schmidl, S., & Skou, N. (2004). Characterizing the dependence of vegetation model parameters on crop structure, incidence angle, and polarization at L-band. *IEEE Transactions on Geoscience and Remote Sensing*, *42*(2), 416–425. https://doi.org/10.1109/TGRS.2003.817976

Xiao, Z., Liang, S., Wang, J., Chen, P., Yin, X., Zhang, L., & Song, J. (2014). Use of general regression neural networks for generating the GLASS leaf area index product. *IEEE Transactions on Geoscience and Remote Sensing*, *52*(1), 209–223. https://doi.org/10.1109/TGRS.2013.2237780

Xu, X., Medvigy, D., Powers, J. S., Becknell, J. M., & Guan, K. (2016). Diversity in plant hydraulic traits explains seasonal and inter-annual variations of vegetation dynamics in seasonally dry tropical forests. *The New Phytologist*, *212*(1), 80–95. https://doi.org/10.1111/nph.14009

Zweifel, R., Item, H., & Häsler, R. (2000). Stem radius changes and their relation to stored water in stems of young Norway spruce trees. *Trees - Structure and Function*, *15*(1), 50–57. https://doi.org/10.1007/s004680000072

Zweifel, R., Item, H., & Häsler, R. (2001). Link between diurnal stem radius changes and tree water relations. *Tree Physiology*, *21*(12-13), 869–877. https://doi.org/10.1093/treephys/21.12-13.869